RMetS

Royal Meteorological Society

A cyclone climatology of the British-Irish Isles 1871–2012

T. Matthews,[a]* C. Murphy,[b] R. L. Wilby[c] and S. Harrigan[b]

[a] *School of Natural Sciences and Psychology, Liverpool John Moore's University, Liverpool L33AF, England, UK*
[b] *Irish Climate Analysis and Research Units (ICARUS), Department of Geography, National University of Ireland Maynooth, Ireland*
[c] *Department of Geography, Loughborough University, LE11 3TU, England, UK*

ABSTRACT: The British-Irish Isles (BI) lie beneath the North Atlantic storm track year-round and thus are impacted by the passage of extra-tropical cyclones. Given recent extreme storminess and projections of enhanced winter cyclone activity for this region, there is much interest in assessing the extent to which the cyclone climate of the region may be changing. We address this by assessing a 142-year (1871–2012) record of cyclone frequency, intensity and 'storminess' derived from the 20th Century Reanalysis V2 (20CR) dataset. We also use this long-term record to examine associations between cyclone activity and regional hydroclimate. Our results confirm the importance of cyclone frequency in driving seasonal precipitation totals which we find to be greatest during summer months. Cyclone frequency and storminess are characterized by pronounced interannual and multi-decadal variability which are strongly coupled to atmospheric blocking in the Euro-Atlantic region, but we detect no evidence of an increasing trend. We observe an upward trend in cyclone intensity for the BI region, which is strongest in winter and consistent with model projections, but promote caution interpreting this given the changing data quality in the 20CR over time. Nonetheless, we assert that long-term reconstruction is helpful for contextualizing recent storminess and for identifying emerging changes in regional hydroclimate linked to cyclones.

KEY WORDS   cyclone; storm; 20th Century Reanalysis; North Atlantic storm track; North Atlantic Oscillation; British-Irish Isles precipitation

Received 11 December 2014; Revised 2 May 2015; Accepted 29 May 2015

1. Introduction

Extra-tropical cyclones are of tremendous physical and societal importance due to their role in redistributing heat, moisture and momentum between latitudes and the extreme surface weather events associated with their passing. The climatological significance of cyclones (or 'storms') is particularly apparent for the British-Irish Isles (BI) as the North Atlantic storm track crosses these densely populated islands year-round (Woollings, 2010). Producing long-term cyclone climatologies for this region has, therefore, attracted attention from the research community (e.g. Sweeney, 2000; Hanna *et al.*, 2008; Allan *et al.*, 2009; Hickey, 2003, 2011; Cornes and Jones, 2011), not least because this area of the North Atlantic is projected to experience enhanced winter cyclone activity as the climate warms (Woollings *et al.*, 2012; Collins *et al.*, 2013; Feser *et al.*, 2014 and references therein). Long-series of observed cyclonicity provide a means to contextualize apparently 'extreme' seasonal storminess (e.g. Blackburn *et al.*, 2008; Dong *et al.*, 2013a; Matthews *et al.*, 2014) as well as to benchmark emerging trends.

Some long-term cyclone climatologies for Europe and/or the BI have used extreme wind speeds as a proxy for storminess, derived from direct surface observations (e.g. Sweeney, 2000; Hickey, 2003, 2011) or geostrophic principles applied to air pressure records (Alexandersson *et al.*, 1998, 2000; Matulla *et al.*, 2008; Wang *et al.*, 2009; Cornes and Jones, 2011). Others have scrutinized high-frequency air pressure variability (Hanna *et al.*, 2008; Allan *et al.*, 2009), or have used tide gauge data (Woodworth and Blackman, 2002; Vilibic and Sepic, 2010; Esteves *et al.*, 2011) to assess historic storminess. Thus, existing work has relied largely upon *in situ* measurements from long-running weather/oceanographic stations to serve as a proxy for cyclone frequency and intensity. Feature identification/tracking algorithms which detect cyclones from gridded pressure fields offer scope for identifying and characterizing cyclones explicitly. Such techniques have yielded cyclone climatologies of the North Atlantic and beyond (Simmonds and Keay, 2000; Wang *et al.*, 2006; Raible *et al.*, 2008), but have rarely been used to gain insight into the cyclone climatology of the BI in particular. Historically, this is explained by the brevity of reanalysis products (∼50 years) compared with station data.

However, the advent of the 20th Century Reanalysis V2 dataset (hereafter 20CR: Compo *et al.*, 2011) permits storm reconstruction back to the 1870s. For example, Wang *et al.* (2013) used the 20CR to identify cyclones over the extra-tropics in both hemispheres, whilst Jones *et al.* (2013) used this dataset to produce an objective catalogue of Lamb weather types (LWTs) for the BI. In addition, Wang *et al.* (2014) presented a 'Cyclone Activity Index'

---

* Correspondence to: Dr. T. Matthews, School of Natural Sciences and Psychology, Liverpool John Moore's University, Liverpool L33AF, England, UK. E-mail: T.R.Matthews@ljmu.ac.uk

(defined in Section 4), and a time series of extreme wind speeds for the North Sea region. Despite the potential that 20CR offers for providing insights into long-term cyclone characteristics (Cornes, 2014), it has not yet been used to construct a cyclone climatology for the BI. We address this gap and seek to complement and extend long-running storminess metrics provided by station-based methods.

2. Aims and objectives

Our main aim is to derive a long-term cyclone record for the BI based on 20CR. Our objectives are to (1) establish the seasonal climatology of cyclones over the region, including their influence on precipitation totals; and (2) explore interannual variations in cyclone activity for the study area linked to large-scale atmospheric circulation.

We pursue objective 1 because despite the recognized role of cyclones as an important feature of the BI climate, and of precipitation and flood frequency in particular (Allan *et al.*, 2009; Pattison and Lane, 2012; Wilby and Quinn, 2013), relatively little attention has been directed towards their seasonal characteristics, or influence on surface climate. In constructing the longest direct record of BI cyclonicity to-date, our study is well placed to make a contribution in this regard. Objective 2 is addressed because changes in cyclone activity over the region and their drivers are of the utmost societal concern. Our study allows emergent cyclone properties to be viewed in the context of a 142-year period, facilitating assessment of low-frequency variations in cyclone activity and the role of wider-scale atmospheric processes in driving cyclone activity.

The following sections provide details of the data (Section 3) and methods (Section 4) used in our study, before proceeding to the results in Section 5. There we outline the role of cyclones within the regional hydroclimate (Section 5.1) and interpret the temporal variability in cyclone activity, including coupling to larger scale atmospheric processes (Section 5.2). These results are then discussed in Section 6 and conclusions are drawn in Section 7.

3. Data

3.1. The 20th Century Reanalysis V2

The 20CR project is described in detail by Compo *et al.* (2011). Briefly, the product provides a comprehensive tropospheric reanalysis spanning the period 1871–2012 at $2° × 2°$ spatial resolution, based on a 56-member ensemble using only observations of surface air pressure, sea surface temperatures and sea ice extent. Uncertainty in the reanalysis is quantified by the spread among ensemble members. Here, 20CR data were extracted for each ensemble member at 6-h resolution (1871–2012: provided by National Oceanic and Atmospheric Administration (NOAA)/Oceanic and Atmospheric Research (OAR)/ Earth System Research Laboratory (ESRL) Physical Sciences Division (PSD) available at http://www.esrl. noaa.gov/psd/) for the BI domain (50°–60°N, 16°W–6°E) used by Matthews *et al.* (2014).

Whilst the accuracy of 20CR is described as equivalent to contemporary 3-day numerical weather predictions, quality in the earlier part of the record has been questioned in assessments of storminess, particularly for data-sparse periods and regions (Wang *et al.*, 2013; Krueger *et al.*, 2014). In particular, variations in the number of observations assimilated into the 20CR through time challenges the identification of trends in storm activity (Section 4.2), as detected changes may be a spurious consequence of changing data quality (Wang *et al.*, 2013). However, previous research suggests that the 20CR is most likely of good quality and homogeneous throughout the BI region (Matthews *et al.*, 2014; Wang *et al.*, 2014). Figure 1 shows that data quality over the BI and Western Europe is less uncertain and quality degrades relatively little earlier in the record, compared with the mid/high-latitude Northern Hemisphere as a whole. Thus, our domain is amongst the most stable regions and, therefore, amenable to producing a robust, long-term cyclone climatology from the 20CR.

3.2. LWTs and precipitation

To corroborate our 20CR cyclone climatology, we compared cyclone counts with the number of pure and hybrid cyclonic LWTs classified objectively by Jones *et al.* (2013) centred on the BI using the 20CR for the period 1871–1947, and the National Centers for Environmental Prediction/National Centre for Atmospheric Research Reanalysis (NCEP/NCAR: Kalnay *et al.*, 1996) for the period 1948–present. The cyclonic LWTs are a useful comparison for our counts because the former have a long legacy in regional climatology (Lamb, 1972) and the Jones *et al.* (2013) version of the catalogue employed here has already demonstrated wider utility in hydrological assessment for the BI back to the 19th Century (e.g. Wilby and Quinn, 2013). We refer to pure and hybrid cyclonic LWTs following the terminology of Lamb (1972), whereby hybrids are those which are a mix of pure synoptic (in this case cyclonic) and directional circulations (e.g. northwest). Objective rules for determining the LWTs are based on geostrophic flow strength/direction and relative vorticity; a description of this scheme can be found in Jones *et al.* (1993, 2013).

In exploring seasonal cyclone climatologies, we assessed the correlation between cyclone metrics and rainfall totals in the gridded CRU TS3.21 dataset (Harris *et al.*, 2014) which covers the period 1901–2012 at $0.5° × 0.5°$ spatial resolution. We also use the long-running England and Wales Precipitation (EWP) record (Alexander and Jones, 2001) to assess any association between years of extreme cyclone activity and precipitation.

To determine links between large-scale atmospheric processes and interannual variability in cyclonicity, we used three indices to describe atmospheric flow in the North Atlantic region: the North Atlantic Oscillation Index (NAOI: Hurrell, 1995), Greenland Blocking Index (GBI: Fang, 2004) and the Blocking Index of Tibaldi and Molteni (1990), extended to two dimensions (Scherrer *et al.*, 2006), and hereafter referred to as BITM. This index identifies
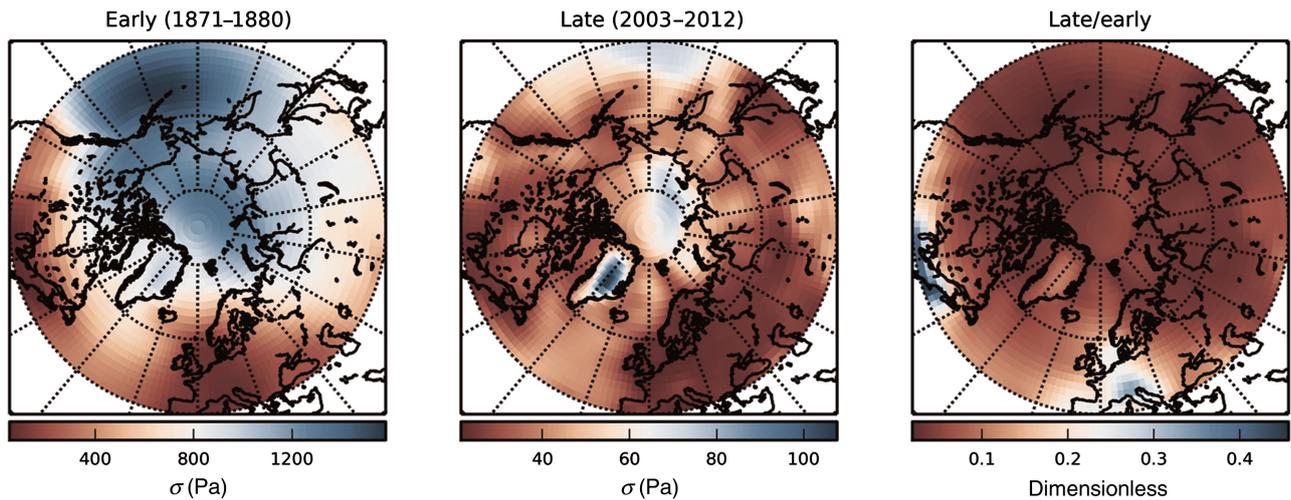
Figure 1. (a and b) Decadal mean standard deviation of daily mean sea-level pressure amongst the 56 20CR ensemble members for the respective decades. To produce these fields, the standard deviation of the daily mean sea-level pressure was calculated across the 56 ensemble members at each grid cell. Time averages for these fields were then calculated for each grid cell and respective decade. (c)Data in the middle panel as a fraction of that plotted in (a). The larger the fraction, the less uncertainty has changed with time implying greater homogeneity in those regions.

blocks by a meridional reversal of the normal poleward geopotential height gradient at the 500 hPa level. The GBI and BITM were thus calculated using the height field of the 500 hPa surface extracted from the 20CR at monthly and daily resolution, respectively. Two versions of the NAOI were used: a principal component (PC) series, derived from the monthly mean 20CR sea-level pressure fields, and the station-based index (data provided by the Climate Analysis Section, NCAR available at: https://climatedataguide.ucar.edu/climate-data/hurrell-north-atlantic-oscillation-nao-index-station-based).

4. Methods

4.1. Cyclone identification and metrics

Following Matthews *et al.* (2014), cyclones were identified using an objective algorithm: an implementation of the Serreze and Barrett (2008) scheme for a regular latitude/longitude grid. The technique classifies cyclones based on the local Laplacian of sea-level pressure. As in Matthews *et al.* (2014), we apply a threshold criterion that a sea-level pressure gradient of at least 1 hPa 250 km^{-1} must be present between a low centre and surrounding cells to qualify as a cyclone.

The algorithm was applied by scanning each 6-h grid from the 56 ensemble members separately. When a cyclone is identified, the location (lat/lon) of the cyclone centre and local Laplacian (intensity: L) are stored. Three cyclone metrics for the BI domain were tallied at seasonal resolution: cyclone counts ($C_{i,j}$), which are simply the number of cyclone centres observed in all grids during year i and season j (note that this measure is equivalent to the 'cyclone centre count' as defined in Neu *et al.*, 2013); mean cyclone intensity ($\overline{L_{i,j}}$)z calculated as the arithmetic mean of the local Laplacians for the $C_{i,j}$ cyclones; and the Cyclone Activity Index (CAI: Wang *et al.*, 2006), given

by $\text{CAI}_{i,j} = C_{i,j} \overline{L}_{i,j}$. The CAI thus weights total counts by mean cyclone intensity. Note that the Laplacian is equivalent to the geostrophic relative vorticity around the cyclone centre and is, therefore, an indicator of low-level convergence. We follow the terminology of Matthews *et al.* (2014) and refer to the CAI as 'storminess' hereafter. Metrics were calculated for each of the 56 ensemble members and then averaged to produce an ensemble-mean series. Seasons were defined as successive 3-month blocks with winter as December (from previous calendar year) to February.

4.2. Interannual variability in cyclonicity

To assess interannual variability in BI cyclonicity, we calculated trends in cyclone metrics over the 142-year (1871–2012) period and examined periods of enhanced storminess cyclone activity in detail. Trends were defined using the non-parametric Theil–Sen slope estimation method (Theil, 1950; Sen, 1968). This metric gives a robust estimate of linear trend in the presence of outliers by using the median slope from an ensemble of trends calculated between every pair of x–y data coordinates. Trend significance (two-tailed) was assessed using the non-parametric Mann–Kendall test (Mann, 1945; Kendall, 1975). Although we report significance for all statistical tests at the 5% level, these values should be interpreted with caution. There is growing recognition that statistical significance is challenging to establish due to the difficulty of defining a valid null hypothesis in poorly understood physical systems (see Cohn and Lins, 2005), as well as dependency of trend significance on choice of start and end dates (e.g. Murphy *et al.*, 2013).

We also recommend that trends should be viewed critically. Although reanalysis projects employ a physically consistent and temporally fixed framework for assimilating data, the spatial density of climate observations is not
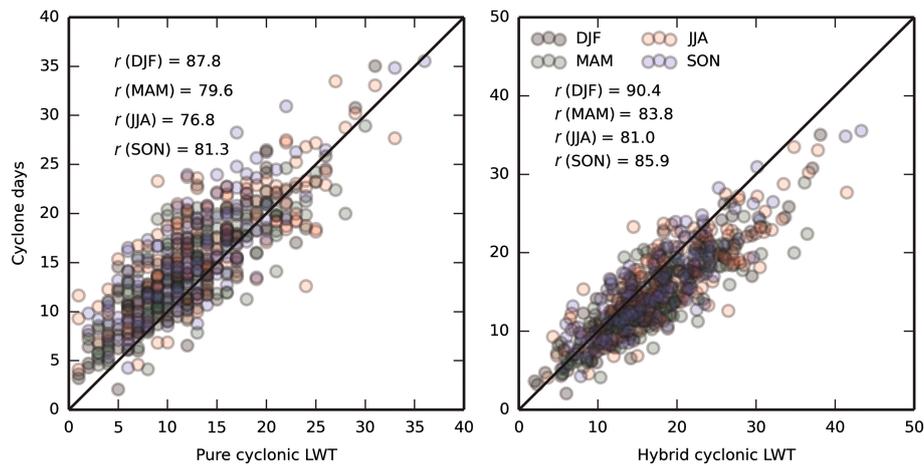
Figure 2. Relationship between 20CR cyclone counts and total pure (left) and hybrid (right) cyclonic LWTs. Seasonal correlation coefficients (multiplied by 100) between series are also shown. Solid black lines denote the 1:1 relationship. 'Cyclone days' is defined as the number of cyclones identified in the 6-h grids, divided by four (to be consistent with the once-daily LWT classification).

constant though time, which means that archives cannot be considered homogeneous (Chang and Fu, 2002; Smits *et al.*, 2005; Hanna *et al.*, 2008). This problem is apparent for reanalysis datasets in general, and can result in spurious variability and trends (Dee *et al.*, 2014). Whilst attempts have been made to correct for inhomogeneities in the 20CR itself (Wang *et al.*, 2013), these corrections are not without a degree of subjectivity, as statistically identified change points used to correct data may reflect legitimate climatic variations. Faced with these complexities, we, therefore, select the simplest and most transparent solution of reporting trends based on raw 20CR data and use the significance as a relative indicator of trend strength. The trend analysis is thus included for completeness and comparison with previous studies. Note that the 20CR has been used in the same unadjusted format for the relatively high-quality data of the BI region by Donat *et al.* (2011), Brönnimann *et al.*, (2012) and Jones *et al.* (2013), with the latter two studies also conducting trend analyses on these unadjusted data.

Individual seasons and spells of enhanced cyclone activity were identified by ranking years and decades according to each cyclone metric. Years characterized as extreme were used to explore the role of wider scale atmospheric processes in driving enhanced cyclone frequency and intensity. This was achieved by compositing standardized 500 hPa height anomalies for those seasons in the top 5% when ranked by the respective cyclone metric (cyclone frequency or intensity). The 500 hPa surface was chosen for analysis as this provides information about atmospheric flow in the mid- and upper-troposphere, permitting insight into the dynamical process generating and steering storms over the North Atlantic.

Linear associations between BI cyclone frequency and intensity with wider scale circulation were explored by calculating Pearson product–moment correlation coefficients between these variables and the NAOI, GBI and BITM. The NAOI was calculated as the monthly time series of the leading empirical orthogonal function of sea-level pressure over the region 20°–80°N, 40°–90°W (e.g. Blessing *et al.*,

2005; Hanna *et al.*, 2014), whilst the GBI was computed as the geopotential monthly height anomaly for the 500 hPa surface over the region 60°–80°N, 20°–80°W (Fang, 2004; Hanna *et al.*, 2013). BITM was calculated for the Atlantic sector (34°–76°N, 84°W–44°E) following the method outlined in Scherrer *et al.* (2006). Unless otherwise stated, all correlations cited below are regarded significant when $p \leq 0.05$.

5. Results

5.1. Cyclone metrics, LWTs and rainfall

Correlations between our (20CR) cyclone counts and total pure and hybrid cyclonic LWTs (Figure 2) are all statistically significant. Correlation strength is generally greater between 20CR and hybrid cyclonic weather types and in winter. 20CR total cyclone counts are higher (lower) than the number of pure (hybrid) cyclonic LWTs, consistent with the findings of Matthews *et al.* (2014) for their winter-only assessment. The overestimation compared to counts of pure cyclonic LWTs may be because we sample the pressure field more frequently (6-h here *vs* 24-h in the LWT analysis), meaning that short-lived lows are more likely to be detected. The fact that the number of hybrid cyclonic LWTs exceeds our cyclone counts could be due to the more stringent definition of a cyclone employed here, which includes an intensity threshold. This may also explain why correlation between LWT counts and our cyclone metrics are weaker outside of winter. Mean cyclone intensity is lower in warmer months and, in the presence of weaker lows, there is evidently a greater chance of disagreement in the detection of a cyclone according to these classification schemes (see below for details of the seasonal cycle in cyclone intensity).

Correlation surfaces for interannual seasonal rainfall variability and cyclone metrics are shown in Figure 3. Correlations between our metrics and rainfall are significant not just for the BI, but for large parts of northwest
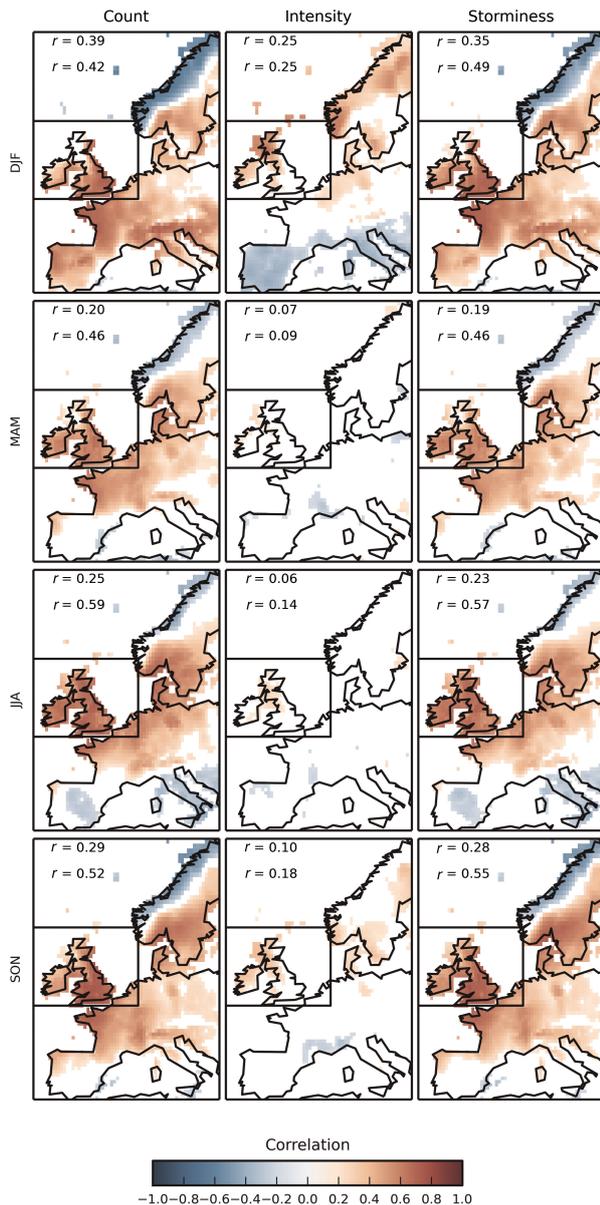
Figure 3. Correlation between gridded CRU TS3.21 precipitation and seasonal cyclone metrics. White areas over land denote where correlations are insignificant ($p > 0.05$). Upper and lower correlation coefficients (r) given in each panel are the mean correlations for the whole domain ($36.25°-69.75°$N, $11.75°$W$-19.75°$E) and BI only, respectively.

Europe. Maps of counts and storminess appear similar because interannual variations in storminess are mainly driven by cyclone counts. This metric has a higher standard deviation than intensity when expressed as a percentage of the mean (C_v of 18.7 vs 6.0%: see Table 1 and Section 5.3) and storminess is calculated with a multiplicative formula (Section 4.1). For conciseness, we focus on the correlation for cyclone counts.

In winter, an area of significant positive correlations with cyclone frequency extends over much of northwest Europe, with the exception of western Scandinavia which registers significant negative correlations. In summer, the area exhibiting significant correlations between the cyclone metrics and precipitation contracts and the

strength of the correlations throughout northern Europe is also generally lower, particularly for western Scandinavia. However, average correlation strength is greatest across the BI during summer and there is a weak spatial gradient in correlation across the domain. This is unlike winter where there is a noteworthy decrease in the strength of the correlation between cyclone count and precipitation with increasing latitude, becoming non-significant for northwest Scotland. In this region, cyclone intensity is significantly correlated with precipitation.

The seasonal regime of cyclone metrics is illustrated in Figure 4. Mean cyclone intensity progresses from a maximum during winter to minimum in summer. The seasonal change in counts is more complex. The probability of cyclone presence over the BI is greatest in late summer (August), with secondary peaks in late spring (May) and late autumn (November). Minimum cyclone frequency occurs in winter. Further insight into this aspect of cyclonicity of the region is provided by Figure 5, where counts are aggregated into 3-month seasons for consecutive 30-year periods (except the abridged period 1991–2012). The summer peak in cyclone frequency is evident again, but interestingly the seasonal maxima is absent from 1961 to 1990. According to Figure 4, the stormiest period for the BI generally occurs in late autumn, as the secondary peak in cyclone frequency combines with the symmetrical cycle in intensity which ascends from the summer minima.

5.2. Interannual variability in BI cyclonicity

Annual and seasonal series of cyclone metrics are shown in Figure 6; coefficients of variation and linear trends are presented in Table 1. Cyclone counts exhibit greatest year-to-year variability. Seasonally, both cyclone frequency and intensity are most variable in winter, with the standard deviation exceeding 40% of the mean for the former. Regarding trends, counts in all seasons have decreased over the period analysed, but the decline is weak and non-statistically significant. Stronger trends are observed for mean cyclone intensity which has increased in all seasons, with the strongest and weakest trends in winter and summer, respectively. The counteracting effects of decreasing cyclone counts with increased mean intensity result in no net change in storminess throughout the period of study: trends for this metric are increasing for all seasons except spring, but all are very weak and statistically insignificant.

The top 7 years (corresponding to ~5% of the record) by cyclone frequency, intensity and storminess are shown in Table 2, while inter-decadal variation in cyclonicity is ranked and illustrated in Figure 7. The stormiest year was 1872 due to high cyclone frequency in winter and autumn. More recently, the years 2000 and 2009 feature as extreme and summer 2012 also registers as exceptional. This extreme seasonal storminess joins the winter of 2013/2014, which Matthews *et al.* (2014) determined as unprecedented since 1871/1872 by updating the winter 20CR BI cyclone series to 2013/2014 using the NCEP

Table 1. Changes in cyclone metrics time series.

	Count (C)		Intensity ($\bar{L}$)		Storminess (CAI)	
	β	C_v	β	C_v	β	C_v
DJF	−0.25 (26.8)	41.7	1.23 (100.0)	13.1	0.67 (55.4)	40.8
MAM	−0.86 (74.7)	33.2	0.67 (99.4)	10.5	−0.19 (22.8)	36.5
JJA	−0.41 (42.4)	33.1	0.42 (92.6)	10.3	0.07 (18.4)	36.5
SON	−0.36 (38.0)	36.6	0.83 (99.9)	11.1	0.35 (34.0)	38.2
Full year	−0.51 (79.8)	18.7	0.75 (100.0)	6.0	0.27 (47.4)	18.9

Trends (β) are given as change per decade in % of the mean over the whole period. Trend significance (in brackets as a percentage) for the corresponding Mann–Kendall statistic (not shown). Coefficients of variation (C_v: mean/standard deviation) are expressed as a percentage.
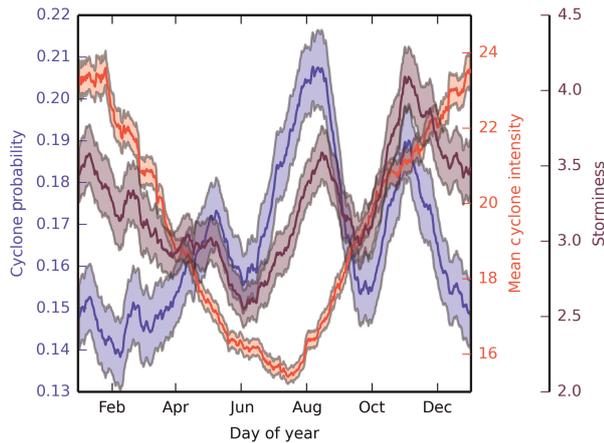

Figure 4. Seasonal variations in cyclone metrics for the BI. All 56 ensemble members' 6-h time series of cyclone counts and intensity were convolved with a 31-day window (with weights equal to the reciprocal of window length). This converts counts to a probability of at least one cyclone being present in the BI domain for the respective time of the year. Storminess was calculated from these smoothed series, expressed as units of probability-weighted intensity; cyclone intensity is in units of Laplacians of sea-level pressure. Smoothed series were averaged over all ensemble members and 142 years (i.e. 1871–2012) to generate the seasonal profiles. Shaded areas denote ±one standard error of the mean; tick marks indicate the beginning of a month.

Figure 5. Mean cyclone counts by season. Bars denote ±one standard error in the ensemble mean for 30-year blocks (except 1991–2012).

reanalysis. The stormiest decade was the 1910s, mainly due to frequent cyclones in winter and spring. The second and third stormiest decades were the 1920s and 1980s, respectively, with the 1920s peak driven by frequent cyclones in spring, summer and autumn, which were also intense in the latter two seasons. The storminess of the 1980s is due to very high cyclone intensity: this decade experienced the most intense cyclones in every season except winter, where it ranked second according to this metric. The quietest decade for storminess was the 1970s on account of the relatively low number of cyclones in spring and summer. The decades of lowest cyclone intensity are mainly found in the earlier part of the record in all seasons, with the 1870s, 1880s and 1890s ranked 14th, 13th and 12th, respectively. This is consistent with the strongly increasing trends found for this metric (Table 1).

5.3. BI cyclonicity and atmospheric circulation

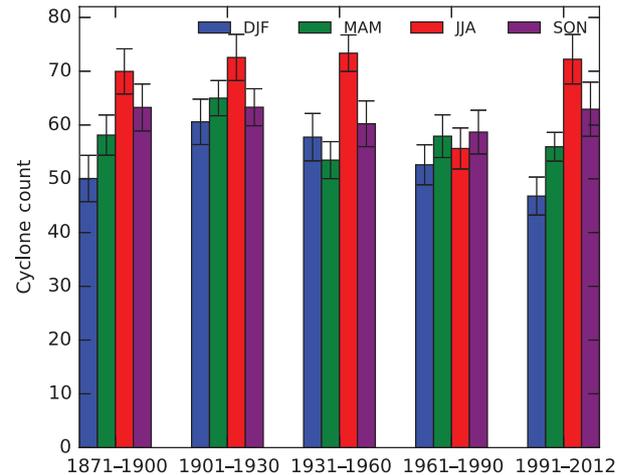To explore how the frequency and intensity of cyclones relate to larger scale atmospheric circulation, we used the years listed in Table 2 to produce composite plots of anomalies at the 500 hPa level (Figure 8). The most coherent anomalies are observed for winter when high cyclone frequency is associated with a low height anomaly over a broad region of the northeast Atlantic, approximately centred over the BI. The downstream anomaly is reminiscent of a Rossby wave train with alternating high/low height anomalies, whilst upstream there is a suggestion of higher geopotential heights in the vicinity of Greenland. A clear geopotential height anomaly signal also emerges in winter when cyclone intensity is considered. Seasons with more intense cyclones are characterized by a height field with positive (negative) anomalies in the low (high) latitudes of the North Atlantic. Outside of winter, coherence in the anomaly field for years of extreme cyclonicity is less evident for both cyclone counts and intensity. In all seasons, more frequent cyclones act to lower geopotential heights in the vicinity of the BI.

To investigate further the link between cyclonicity and larger scale atmospheric circulation, we also determined associations between cyclone metrics and indices of atmospheric circulation in the North Atlantic region. As the BITM is a two-dimensional index, we explore associations between blocking frequency at each grid point and cyclone frequency/intensity (Figure 9). For all seasons, an increase in cyclone frequency for the BI is associated with a decrease in blocking over the
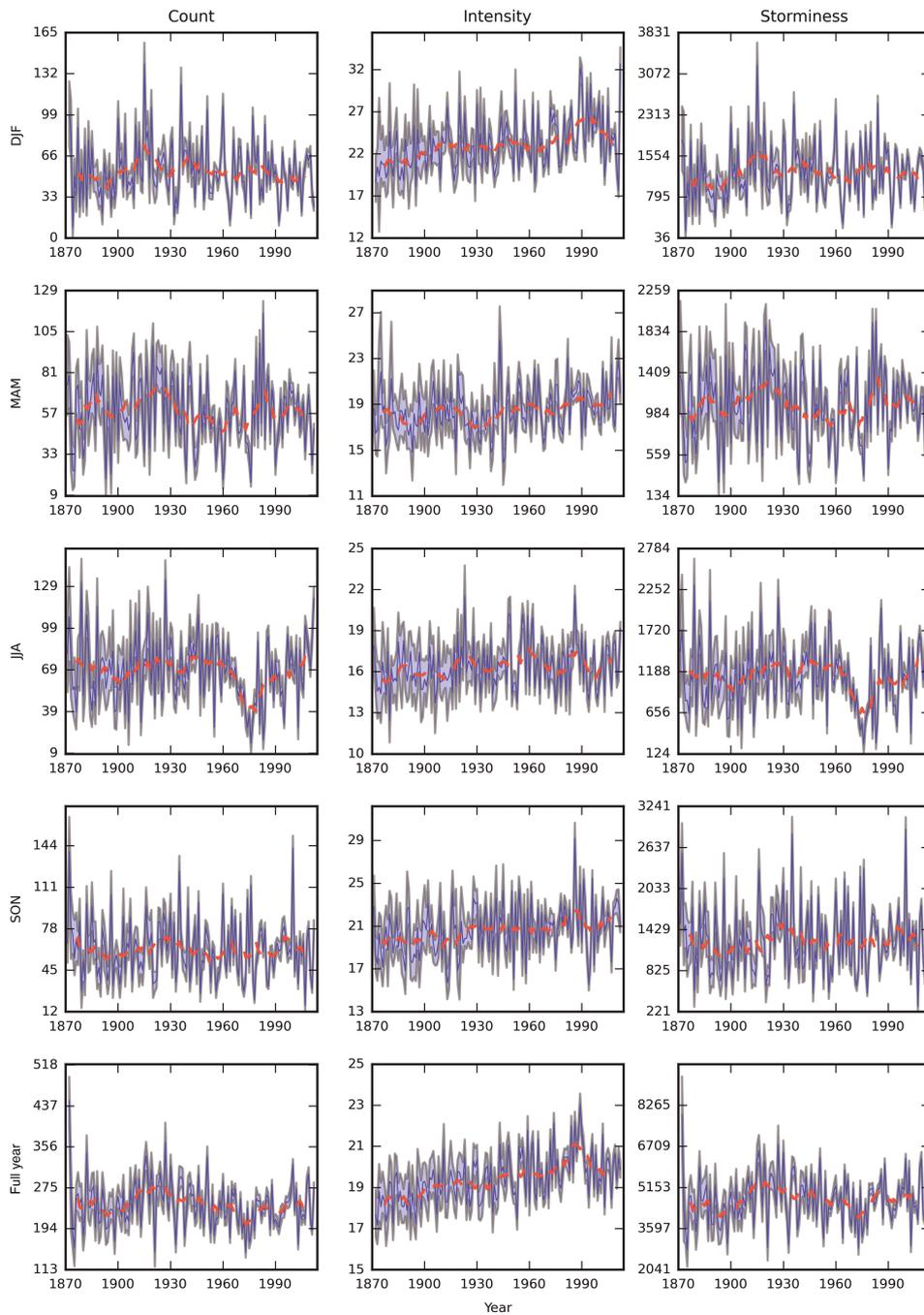
Figure 6. Annual cyclone metrics by season and full year. Solid lines show the ensemble mean and shaded regions span the range of the 56 ensemble members. Dotted lines are the 11-year moving average. Units of count are simply the number of centres detected in the 6-h grids, whilst intensity and storminess have units of Laplacians of mean sea-level pressure.

region and an increase in blocking at higher latitudes over the Atlantic. In winter, the area of significant positive correlations between high-latitude blocking and BI cyclone frequency is relatively extensive, with significant correlations found to the west and east of Greenland. In other seasons, positive correlations only persist to the east. In spring, summer and autumn, cyclone intensity generally exhibits weaker correlations (than frequency) with blocking. During the winter months, cyclones over the BI tend to be more intense when blocking is increased (decreased) to the south (north) of the islands.

Correlations between the cyclone metrics and the NAOI and GBI are provided in Table 3. For comparison, and on the basis of Figure 9, we also report correlations between blocking frequency for the BI domain ($50°–60°N$, $16°W–6°E$; hereafter 'BIBF' – BI Blocking Frequency) and cyclone frequency/intensity. BIBF is defined as the daily probability of at least one grid cell being blocked within the BI domain. The strongest correlations for cyclone counts are observed for BIBF, but significant correlations are similarly apparent between frequency and both the NAOI and GBI. These indices

Table 2. Top seven ranked years (i.e. ~5% of the dataset) for each cyclone metric by season.

Rank	1	2	3	4	5	6	7
Counts							
DJF	1915	1936	1960	1919	1951	1872	1977
MAM	1983	1981	1920	1909	1979	1888	1882
JJA	1927	1879	2012	1888	1912	1917	1882
SON	2000	1872	1935	1976	1960	1896	1974
Full year	1872	1927	1882	1916	1951	2000	1930
Intensity							
DJF	2012	1989	1990	1995	1993	1952	2000
MAM	1943	1982	2011	2007	2002	1963	1919
JJA	1986	1923	1948	1949	1956	1959	1962
SON	1986	1996	1991	1989	1954	1950	1945
Full year	1989	1986	1974	1984	1959	1990	2002
Storminess							
DJF	1915	1984	1936	1960	1910	1919	1900
MAM	1983	1981	1920	1908	1919	1922	1909
JJA	2012	1879	1927	1888	1986	1917	1956
SON	2000	1935	1872	1976	1916	1974	1896
Full year	1872	1927	1916	1930	1951	2000	2009

DJF, December–February; JJA, June–August; MAM, March–May; SON, September–November.
Note that Matthews *et al.* (2014) found that winter of 2013/2014 was the stormiest since 1871/1872, based on NCEP reanalysis for years outside the 1871/1872–2012 period of 20CR.

are also significantly correlated with average cyclone intensity. The results indicate that periods of positive (negative) NAO (GBI) conditions are associated with fewer, but more intense cyclones over the BI. This relationship breaks down somewhat in summer (no significant correlation with cyclone intensity) and autumn (no significant correlation with cyclone frequency), but is otherwise persistent. This is characteristic of the fact that, with the exception of the association between BIBF and counts, correlations between cyclone metrics and circulation indices are generally strongest in the winter.

6. Discussion

6.1. BI cyclonicity and regional hydroclimate

The 142-year record yields new insights into the cyclone climate of the BI. Strong and statistically significant correlations between seasonal precipitation and cyclone frequency confirm the regional hydroclimatic importance of cyclones. The stormiest periods have also been recognized as extreme in other hydroclimatic indicators: e.g. the top-ranking winter (1915) and autumn (2000) are the wettest in the long-running EWP series for the overlapping period (1871/1872–2012), whilst the stormiest spring (1983) and summer (2012) also rank highly (fourth and third, respectively). Extensive seasonal flooding has additionally been documented during periods recognized as extremely stormy: e.g. autumn 2000 (Marsh and Dale, 2002; Jones *et al.*, 2006), and summer 2012 (Dong *et al.*, 2013a; Parry *et al.*, 2013). Moreover, the stormiest year (1872) is wettest in the EWP series and has been noted as a particularly flood-rich period (Jones *et al.*, 2006; Wilby and Quinn, 2013). The most subdued decade in terms of storminess (the 1970s) was a period of exceptional drought in the BI (Jones *et al.*, 2006; Marsh *et al.*,

2007; Rodda and Marsh, 2011; Murphy *et al.*, 2013). Correspondence with independent hydroclimatic indicators highlights the importance of cyclones for the regional hydroclimate, and simultaneously corroborates the 20CR cyclone reconstruction.

Correlation between precipitation and cyclone counts was highest during summer. This differs from Lavers *et al.* (2013), who found that the relationship between mean sea-level pressure (MSLP) and precipitation across northwest Europe (including the BI) was weaker in summer than in winter. One explanation for this discrepancy is that the storm track is known to be more spatially restricted in summer than winter over the northeast Atlantic (Mesquita *et al.*, 2008). Thus, where cyclone frequency is an important driver of precipitation totals, it is reasonable to expect that regions of significant correlations between rainfall totals and MSLP (which bare the imprint of depression passage) should be similarly constrained. The different period (1957–2002) and spatial resolution (2.5° × 2.5°) of the reanalysis dataset used by Lavers *et al.* (2013) could be another factor. In highlighting the importance of cyclones in driving high precipitation amounts over the BI throughout the year, our results agree with Murphy and Washington (2001), who, in all seasons, observed a cyclonic pattern in the correlation field centred on the BI when assessing the association between MSLP and the leading empirical orthogonal function of BI rainfall.

Correlations between summer precipitation and summer cyclone counts are more spatially consistent over BI relative to other seasons. During winter, correlations between cyclone counts/storminess, and precipitation are insignificant for the northwest of our domain where we observed stronger correlations between cyclone intensity and precipitation. Periods of enhanced cyclone intensity for the BI have been associated with positive phases of the NAO (Allan *et al.*, 2009, and see Section 6.2). This
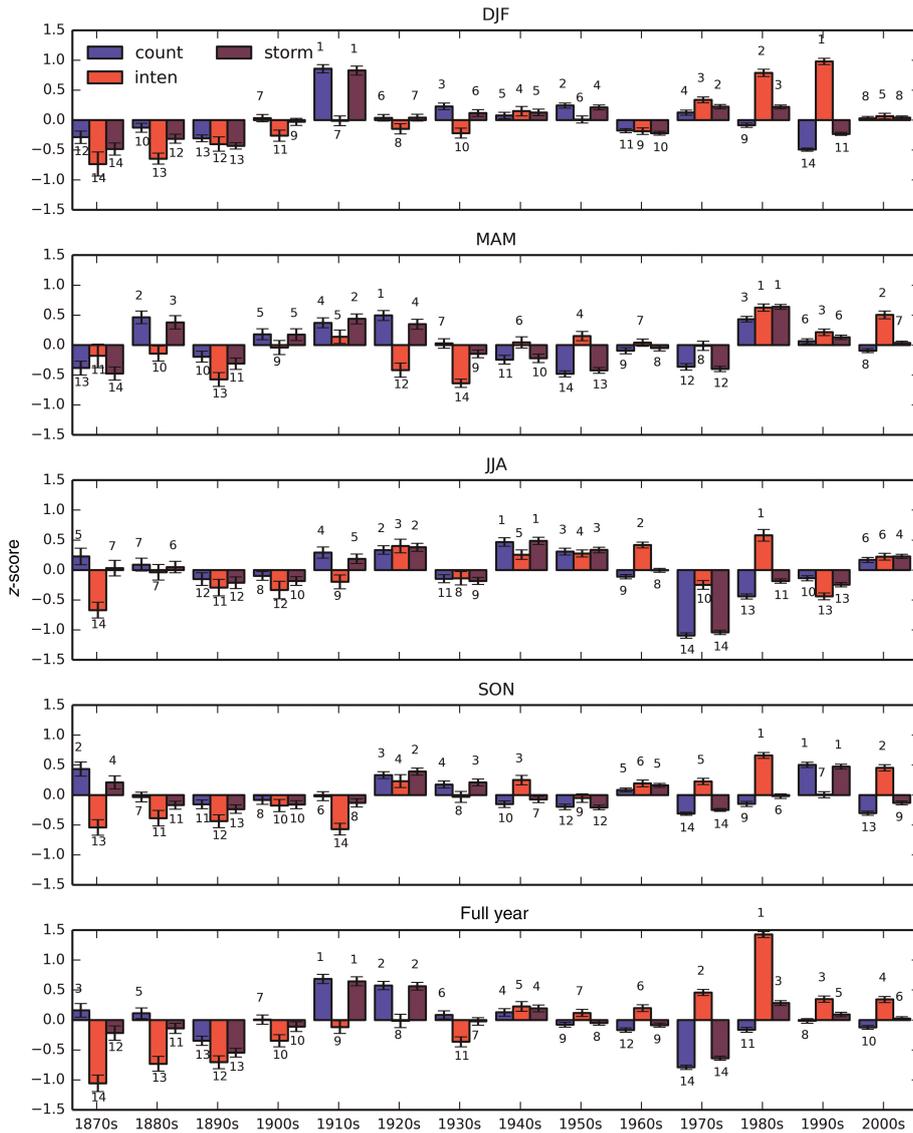
Figure 7. Decadal mean cyclone statistics by season expressed as a *z*-score averaged over all 56 20CR ensemble members. Error bars indicate ±one standard deviation of the 56 decadal means. Numbers above/below the bars give the rank of the decade for the respective metric and season.

correspondence is strongly hinted at in Figure 3 as the correlation between BI cyclone intensity and precipitation mirrors the association between the NAOI and European winter precipitation (Wilby *et al.*, 1997; Trigo *et al.*, 2002), reflecting the more northerly (southerly) position of the storm track during NAO positive (negative) conditions. When cyclones take a more northerly route over the northeast Atlantic, they will not be counted in our BI domain but may still enhance seasonal precipitation in the northwest BI through the passage of trailing fronts. During positive NAO conditions, the stronger westerly flow is also understood to increase orographic rainfall for the British uplands (Burt and Howden, 2013). These mechanisms explain the lack of correlation between cyclone counts and precipitation in the northwest in winter: precipitation can be enhanced in the northwest BI by the passage of 'local' cyclones (which will register in our counts) through low-level convergence and frontal lifting, but also by 'remote' cyclones north of our domain, as both trailing

fronts and enhanced orographic uplift associated with a more northerly storm track are important rainfall generating mechanisms. We suggest that in winter the latter are more important, due to the stronger westerly flow, but that in summer the former emerges as dominant when the westerly flow weakens (cf. Wilby *et al.*, 2002). This would also account for the more spatially homogenous summer correlation field in Figure 3. Regardless of the physical processes driving correlations, cyclone frequency has already been linked to spatially extensive flooding episodes (Wilby and Quinn, 2013) due to high rainfall amounts across the BI associated with cyclone passage (Burt *et al.*, 2014). We emphasize that these conclusions are perhaps most appropriate for summer based on the evidence presented here.

6.2. Atmospheric circulation and temporal variability in BI cyclonicity

Days with cyclonic circulation over the BI are most frequent in summer. This finding is consistent with
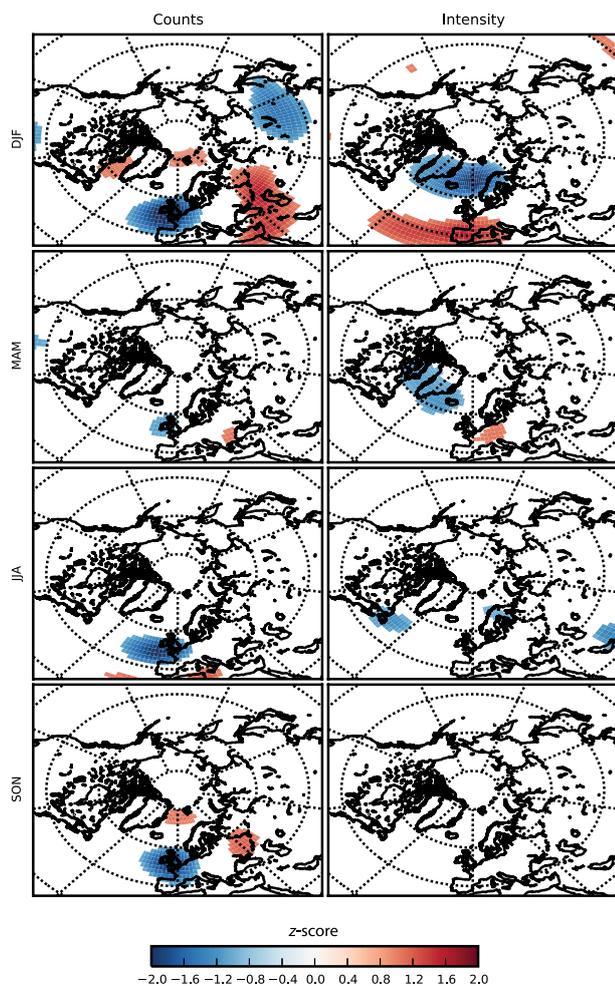
Figure 8. Composite standardized anomalies (*z*-scores) in the 500 hPa geopotential height field for the years of exceptional cyclone frequency (left) and intensity (right) (see Table 2). Grid cells with absolute *z*-scores less than 1 are white.
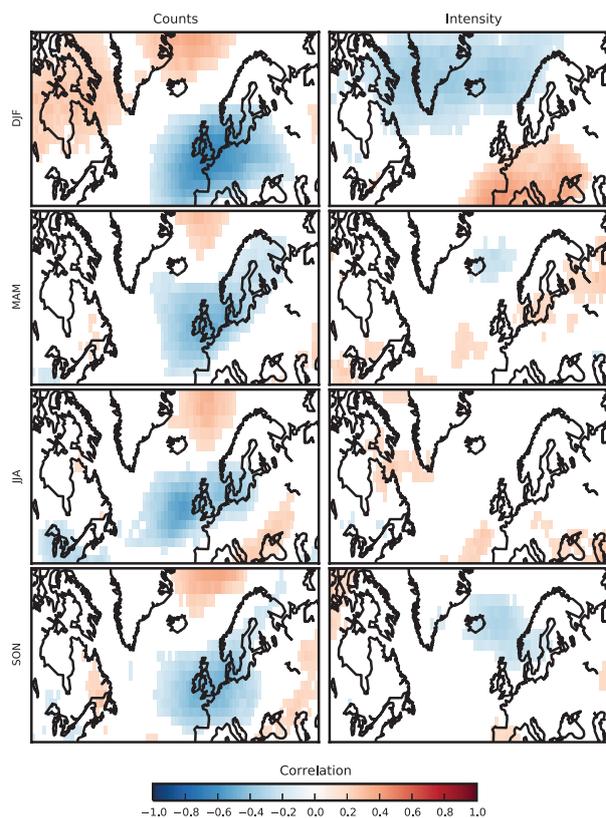

Figure 9. Correlation between blocking frequency (BITM) at each grid point and cyclone frequency (left) and intensity (right) over the BI. Regions where the correlation is significantly different from zero at $p < 0.05$ (according to a two-tailed *t*-test) are shaded.

Mesquita *et al.* (2008) who showed that the northeast North Atlantic is among the few regions in the Northern Hemisphere to experience a summer cyclone maximum. The assessment of cyclonicity (Section 5.4) provides some insight to physical processes driving the seasonal cycle in cyclone frequency. Cyclone counts were found to correlate most strongly with the BIBF, such that increased regional blocking translates into fewer cyclonic circulation days. This fits with the summer-only investigation of Dong *et al.* (2013b) and agrees with the negative correlation between cyclonic and anticyclonic LWTs noted by Burt *et al.* (2014). Figure 10 (left) demonstrates that this relationship generally holds when the seasonal climatological cycle is assessed: the blocking minimum in summer, characteristic of conditions across the north-eastern margin of Europe (Figure 10, right), coincides with the summer cyclone maxima. The relationship between interannual blocking and cyclone frequency is further highlighted by anomalous conditions during the 1961–1990 climate normal period (cf. Section 6.1 and Figure 5), during which the summer cyclone maximum was not observed. This was also a 30-year period characterized by frequent summer

blocking (Table 4). It is interesting to note that a 30-year period (1961–1990) widely used to define climate normals was actually highly unusual from the perspective of summer atmospheric circulation for the BI.

To assess the role of larger scale atmospheric processes modulating BI cyclonicity climate, we correlated cyclone metrics with climate indices. The GBI and NAOI exhibited correlation coefficients that were opposite in sign, which is unsurprising given the association between Greenland blocking and the NAO (Woollings *et al.*, 2008). As correlations were stronger for the NAOI, we focus on this index here. Interannual variability in cyclone frequency was generally found to be negatively correlated with the NAOI in most seasons, the signal being strongest (highest *r* values) using the PC-based NAOI, and in winter. The sign of relationship is consistent with analyses using the cyclonic LWT (e.g. Wilby *et al.*, 1997; Burt *et al.*, 2014). Negative correlation may reflect either slower moving cyclonic systems during NAO negative years (subdued westerly circulation), or the passage of more cyclonic weather systems, as both processes could contribute to a higher number of cyclone days for our domain.

Cyclone intensity was positively correlated with the NAOI in most seasons, with strongest associations in winter, which concurs with Allan *et al.* (2009) and Wang *et al.* (2009, 2011). The relationship between the NAO and cold-season cyclone intensity is also consistent with

Table 3. Correlation between BI cyclone metrics and atmospheric circulation indices.

Season	Cyclone metric	NAO_{pc}	$NAO_{station}$	GBI	BIBF
DJF	Counts	**−0.40**	**−0.20**	**0.33**	**−0.53**
	Intensity	**0.56**	**0.48**	**−0.48**	0.05
MAM	Counts	**−0.27**	−0.11	**0.25**	**−0.65**
	Intensity	**0.26**	**0.19**	**−0.26**	0.05
JJA	Counts	**−0.33**	−0.09	**0.21**	**−0.65**
	Intensity	0.01	0.00	−0.08	0.02
SON	Counts	0.01	0.12	0.13	**−0.68**
	Intensity	**0.29**	**0.23**	**−0.23**	**−0.18**

BIBF denotes the blocking frequency in the BI domain (50°–60°N, 16°W–6°E); 20CR PC and station-based NAO indices are subscripted with $_{pc}$ and $_{station}$, respectively. Correlations in bold are significantly different from zero at $p < 0.05$, according to a two-tailed t-test.
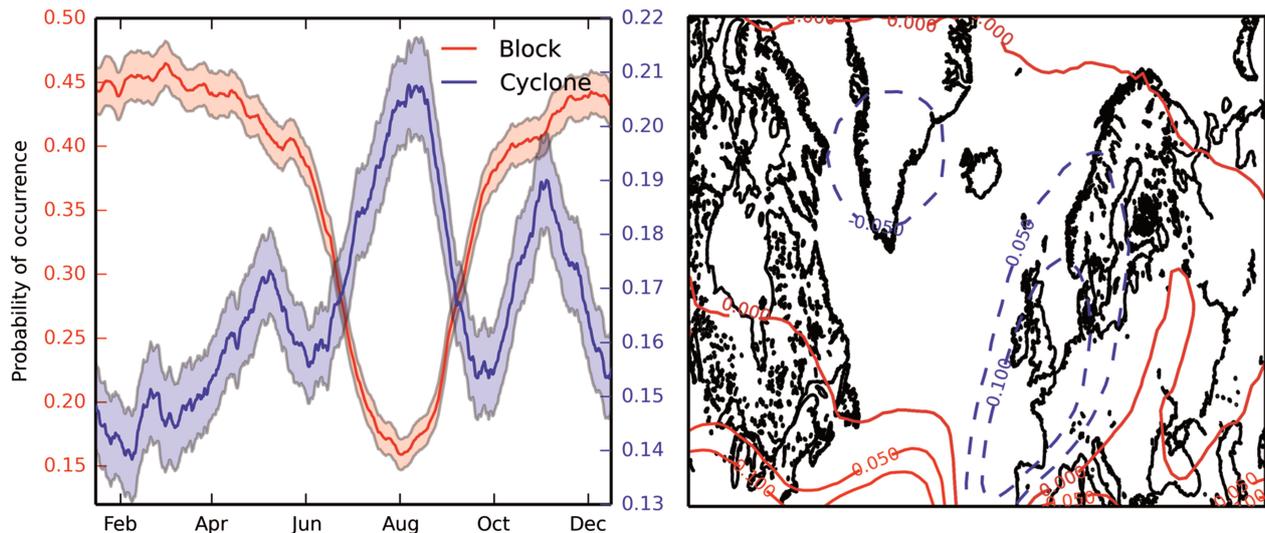

Figure 10. Left: Seasonal cycle of cyclone probability and blocking probability for the BI domain. The cyclone probability curve is taken from Figure 4. The blocking curve is calculated via the same convolution procedure described in Figure 4 caption and represents the probability of at least one grid cell being blocked in the BI domain. Right: Summer minus winter blocking frequency (%) across the North Atlantic region, averaged over the full length of the 20CR.

Table 4. Relative cyclone and blocking frequency for the BI domain in summer for 30-year normal periods (except 1991–2012).

Period	Relative cyclone frequency (%)	Relative blocking frequency (%)
1871–1900	101.8	86.6
1901–1930	105.5	99.8
1931–1960	106.7	100.6
1961–1990	80.9	123.0
1991–2012	105.1	90.1

Here, blocking frequency is calculated according to the definition of the BIBF with percentages derived relative to the long-term (1871–2012) summer mean.

the intense winter storminess identified during the 1990s (exceptionally positive NAO – see Hanna *et al.*, 2014) in this study (Section 5.4) and in previous investigations (Jones *et al.*, 1999; Allan *et al.*, 2009; Wang *et al.*, 2009, 2011; Cornes and Jones, 2011; Donat *et al.*, 2011). Whilst the NAOI exhibits statistically significant correlations with our cyclone metrics, we note that even during winter when these associations are strongest, the NAO only accounts for ∼16 and 31% of the variance in cyclone frequency and intensity, respectively. Thus, the utility of the NAO for interpreting BI cyclonicity is perhaps limited (cf. Burningham and French, 2013).

Our results suggest an increase in cyclone intensity for all seasons over the BI that is strongest in winter. Detailed comparison with other research is confounded by differences in the choice of metrics, domains and sampling resolutions. However, increased BI cyclone intensity is broadly supported by investigations of trends in extreme wind speeds using the 20CR (Donat *et al.*, 2011; Brönnimann *et al.*, 2012) and by Wang *et al.* (2013) who found increasing mean Laplacian from the 20CR for the high-latitude North Atlantic (in which our domain is mostly situated). These results stand in contrast with studies using *in situ* pressure observations to determine changes in BI cyclone intensity (e.g. Hanna *et al.*, 2008; Wang *et al.*, 2009, 2011). Although such contradictions regarding the 20CR has been raised before (Krueger *et al.*, 2014; Wang *et al.*, 2014), the cause remains unclear. Improved understanding of this disagreement is needed as enhanced cold-season cyclone intensity has been projected for the BI region (Collins

et al., 2013; Zappa *et al.*, 2013; Feser *et al.*, 2014). Robust long-term cyclone climatologies are required if emerging trends are to be differentiated from natural variability.

Cyclone frequency and storminess were more closely related to interannual variation in BI precipitation. Recent years have seen three of the stormiest seasons on record, with autumn (2000) and summer (2012) joining the winter of 2013/2014 [see Matthews *et al.* (2014)] as the most exceptional seasons since the beginning of 20CR. Despite this clustering, we detected no evidence for an upward trend in storminess, reflecting the signal (or lack of) in cyclone frequency compared to the noise of interannual variability. However, pronounced, low-frequency variability in these metrics is evident, which underscores the utility of the long-term cyclone climatology presented here in contextualizing recent extremes. For example, the highly subdued storminess observed during the 1961–1990 climate normal period has perhaps made the return to more typical conditions in recent years seem unusual. Trends with start dates during this quiescent period are likely to be misleading: calculating the Mann–Kendall test statistic on the period 1979–2012 [the period of satellite observation that signals the start date of the ERA-Interim Reanalysis dataset: Dee *et al.* (2011)], yields upward trends in summer cyclone frequency and storminess with *p*-values of 0.017 and 0.044, respectively. Thus, despite the higher quality of more recent gridded data products for objective assessment of atmospheric circulation, there remains a need for the longer term perspective afforded by products such as the 20CR is clear.

7.   Conclusions

We have constructed a 142-year cyclone climatology for the BI using the 20CR. This product both confirms and clarifies the importance of cyclones to the hydroclimate of this region. Seasonal precipitation totals were found to be strongly correlated with cyclone frequency across large parts of the BI, but this is most apparent during the summer, when these weather types are more frequent. We therefore conclude that any changes in the frequency of 'local' cyclones for the region would be particularly important for seasonal precipitation totals during summer. In this context, we detected no trend in cyclone frequency or storminess in any season, but did establish that the 1961–1990 climate normal was extraordinary for the rarity of summer cyclones, which is consistent with the severe droughts reported for the same period. Such low-frequency variability in cyclone frequency was found to be strongly associated with atmospheric blocking – a control which also emerged when the seasonal cycle in this metric was assessed. Thus, we emphasize that to better understand the processes driving variability in the frequency of cyclones for the BI, it is necessary to investigate mechanisms that modulate atmospheric blocking in the Euro-Atlantic sector.

Cyclone intensity was observed to be significantly correlated (positive) with the NAOI, particularly in winter,

which is generally in agreement with the literature. However, our detection of a strong upward trend in cyclone intensity highlights a discrepancy between long-term reanalysis reconstructions and assessments of cyclone intensity based on station data. Given expectations of enhanced cyclone activity for the BI in a warmer climate, we emphasize that resolving this matter should be a high priority for future research.

References

Alexander LV, Jones PD. 2001. Updated precipitation series for the UK and discussion of recent extremes. *Atmos. Sci. Lett.* **1**: 142–150.

Alexandersson H, Schmith T, Iden K, Tuomenvirta H. 1998. Long-term variations of the storm climate over NW Europe. *Glob. Atmos. Ocean Syst.* **6**: 97–120.

Alexandersson H, Tuomenvirta H, Schmith T, Iden K. 2000. Trends of storms in NW Europe derived from an updated pressure data set. *Clim. Res.* **14**: 71–73.

Allan R, Tett S, Alexander L. 2009. Fluctuations in autumn–winter severe storms over the British Isles: 1920 to present. *Int. J. Climatol.* **29**: 357–371.

Blackburn M, Methven J, Roberts N. 2008. Large-scale context for the UK floods in summer 2007. *Weather* **63**: 280–288.

Blessing S, Fraedrich K, Junge M, Kunz T, Lunkeit F. 2005. Daily North-Atlantic Oscillation (NAO) index: statistics and its stratospheric polar vortex dependence. *Meteorol. Z.* **14**: 763–769.

Brönnimann S, Martius O, Von Waldow H, Welker C, Luterbacher J, Compo GP, Sardeshmukh PD, Usbeck T. 2012. Extreme winds at northern mid-latitudes since 1871. *Meteorol. Z.* **21**: 13–27.

Burningham H, French J. 2013. Is the NAO winter index a reliable proxy for wind climate and storminess in northwest Europe? *Int. J. Climatol.* **33**: 2036–2049.

Burt TP, Howden NJK. 2013. North Atlantic Oscillation amplifies orographic precipitation and river flow in upland Britain. *Water Resour. Res.* **49**: 3504–3515.

Burt TP, Jones PD, Howden NJK. 2014. An analysis of rainfall across the British Isles in the 1870s. *Int. J. Climatol.*, doi: 10.1002/joc.4184.

Chang EKM, Fu Y. 2002. Interdecadal variations in Northern Hemisphere winter storm track intensity. *J. Clim.* **15**: 642–658.

Cohn TA, Lins HF. 2005. Nature's style: naturally trendy. *Geophys. Res. Lett.* **32**: L23402.

Collins M, Knutti R, Arblaster J, Dufresne J-L, Fichefet T, Friedlingstein P, Gao X, Gutowski WJ, Johns T, Krinner G, Shongwe M, Tebaldi C, Weaver AJ, Wehner M. 2013. Long-term climate change: projections, commitments and irreversibility. In *Climate Change 2013: The Physical Science Basis. Contribution of Working Group I to the Fifth Assessment Report of the Intergovernmental Panel on Climate Change*, Stocker TF, Qin D, Plattner G-K, Tignor M, Allen SK, Boschung J, Nauels A, Xia Y, Bex V, Midgley PM (eds). Cambridge University Press: Cambridge, UK and New York, NY.

Compo GP, Whitaker JS, Sardeshmukh PD, Matsui N, Allan RJ, Yin X, Gleason BE, Vose RS, Rutledge G, Bessemoulin P, Brönnimann S, Brunet M, Crouthamel RI, Grant AN, Groisman PY, Jones PD, Kruk MC, Kruger AC, Marshall GJ, Maugeri M, Mok HY, Nordli Ø, Ross TF, Trigo RM, Wang XL, Woodruff SD, Worley SJ. 2011. The Twentieth Century Reanalysis Project. *Q. J. R. Meteorol. Soc.* **137**: 1–28.

Cornes RC. 2014. Historic storms of the northeast Atlantic since circa 1700: a brief review of recent research. *Weather* **69**: 121–125.

Cornes RC, Jones PD. 2011. An examination of storm activity in the northeast Atlantic region over the 1851–2003 period using the EMULATE gridded MSLP data series. *J. Geophys. Res.* **116**: D16110.

Dee DP, Uppala SM, Simmons AJ, Berrisford P, Poli P, Kobayashi S, Andrae U, Balmaseda MA, Balsamo G, Bauer P, Bechtold P, Beljaars ACM, Van de Berg L, Bidlot J, Bormann N, Delsol C, Dragani R, Fuentes M, Geer AJ, Haimberger L, Healy SB, Hersbach H, Hólm EV, Isaksen L, Kållberg P, Köhler M, Matricardi M, Mcnally AP, Monge-sanz BM, Morcrette J, Park B, Peubey C, de Rosnay P, Tavolato C, Thépaut J, Vitart F. 2011. The ERA-Interim reanalysis: configuration and performance of the data assimilation system. *Q. J. R. Meteorol. Soc.* **137**: 553–597.

Dee D, Fasullo J, Shea D, Walsh J, National Center for Atmospheric Research Staff (eds). 2014. *The climate data guide*: *atmospheric*

reanalysis: *overview & comparison tables*. https://climatedataguide.ucar.edu/climate-data/atmospheric-reanalysis-overview-comparison-tables (accessed 5 November 2014).

Donat MG, Renggli D, Wild S, Alexander LV, Leckebusch GC, Ulbrich U. 2011. Reanalysis suggests long-term upward trends in European storminess since 1871. *Geophys. Res. Lett.* **38**: L14703.

Dong B, Sutton R, Woolings T. 2013a. The extreme European Summer 2012 [in "Explaining Extreme Events of 2012 from a Climate Perspective]. *Bull. Am. Meteorol. Soc.* **9**: s28–s32.

Dong B, Sutton RT, Woollings T, Hodges K. 2013b. Variability of the North Atlantic summer storm track: mechanisms and impacts on European climate. *Environ. Res. Lett.* **8**: 034037.

Esteves LS, Williams JJ, Brown JM. 2011. Looking for evidence of climate change impacts in the eastern Irish Sea. *Nat. Hazards Earth Syst.* **11**: 1641–1656.

Fang ZF. 2004. Statistical relationship between the northern hemisphere sea ice and atmospheric circulation during wintertime. In *Observation, Theory and Modeling of Atmospheric Variability*. World Scientific Series on Meteorology of East Asia, Zhu X (ed). World Scientific Publishing Company: Singapore, 131–141.

Feser F, Barcikowska M, Krueger O, Schenk F, Weisse R, Xia L. 2014. Storminess over the North Atlantic and northwestern Europe – a review. *Q. J. R. Meteorol. Soc.* **141**: 350–382.

Hanna E, Cappelen J, Allan R, Jónsson T, Le Blancq F, Lillington T, Hickey K. 2008. New insights into North European and North Atlantic surface pressure variability, storminess, and related climatic change since 1830. *Int. J. Climatol.* **21**: 6739–6766.

Hanna E, Jones JM, Cappelen J, Mernild SH, Wood L, Steffen K, Huybrechts P. 2013. The influence of North Atlantic atmospheric and oceanic forcing effects on 1900–2010 Greenland summer climate and ice melt/runoff. *Int. J. Climatol.* **33**: 862–880.

Hanna E, Cropper TE, Jones PD, Scaife AA, Allan R. 2014. Recent seasonal asymmetric changes in the NAO (a marked summer decline and increased winter variability) and associated changes in the AO and Greenland Blocking Index. *Int. J. Climatol.*, doi: 10.1002/joc.4157.

Harris I, Jones PD, Osborn TJ, Lister DH. 2014. Updated high-resolution grids of monthly climatic observations – the CRU TS3.10 Dataset. *Int. J. Climatol.* **34**: 623–642.

Hickey KR. 2003. The storminess record from Armagh Observatory 1796-1999. *Weather* **58**: 28–35.

Hickey KR. 2011. The hourly gale record from Valentia Observatory, SW Ireland 1874-2008 and some observations on extreme wave heights in the NE Atlantic. *Clim. Change* **106**: 483–506.

Hurrell JW. 1995. Decadal trends in the North Atlantic Oscillation: regional temperatures and precipitation. *Science* **269**: 676–679.

Jones PD, Hulme M, Briffa KR. 1993. A comparison of Lamb circulation types with an objective classification scheme. *Int. J. Climatol.* **13**: 655–663.

Jones PD, Horton EB, Folland CK, Hulme M, Parker DE, Basnett TA. 1999. The use of indices to identify changes in climatic extremes. *Clim. Change* **42**: 131–149.

Jones PD, Lister DH, Wilby RL, Kostopoulou E. 2006. Extended river flow reconstructions for England and Wales, 1865-2002. *Int. J. Climatol.* **26**: 219–231.

Jones PD, Harpham C, Briffa KR. 2013. Lamb weather types derived from reanalysis products. *Int. J. Climatol.* **33**: 1129–1139.

Kalnay E, Kanamitsu M, Kistler R, Collins W, Deaven D, Gandin L, Iredell M, Saha S, White G, Woollen J, Zhu Y, Leetmaa A, Reynolds R, Chelliah M, Ebisuzaki W, Higgins W, Janowiak J, Mo KC, Ropelewski C, Wang J, Jenne R, Joseph D. 1996. The NCEP/NCAR 40-year reanalysis project. *Bull. Am. Meteorol. Soc.* **77**: 437–471.

Kendall MG. 1975. *Rank Correlation Methods*. Charles Griffin: London.

Krueger O, Feser F, Bärring L, Kaas E, Schmith T, Tuomenvirta H, von Storch H. 2014. Comment on trends and low frequency variability of extra-tropical cyclone activity in the ensemble of twentieth century reanalysis by Xiaolan L. Wang, Y. Feng, GP Compo, VR Swail, FW Zwiers, RJ Allan, and PD Sardeshmukh, Climate Dynamics, 2012. *Clim. Dyn.* **42**: 1127–1128.

Lamb HH. 1972. British Isles weather types and a register of daily sequence of circulation patterns, 1861-1971. Geophysical Memoir 116, HMSO, London.

Lavers D, Prudhomme C, Hannah DM. 2013. European precipitation connections with large-scale mean sea-level pressure (MSLP) fields. *Hydrol. Sci. J.* **58**: 310–327.

Mann HB. 1945. Nonparametric tests against trend. *Econometrica* **13**: 245–259.

Marsh TJ, Dale M. 2002. The UK floods of 2000–2001: a hydrometeorological appraisal. *Water Environ. J.* **16**: 180–188.

Marsh T, Cole G, Wilby RL. 2007. Major droughts in England and Wales, 1800-2006. *Weather* **62**: 87–93.

Matthews T, Murphy C, Wilby RL, Harrigan S. 2014. Stormiest winter on record for Ireland and UK. *Nat. Clim. Change* **4**: 738–740.

Matulla C, Schöner W, Alexandersson H, Von Storch H, Wang XL. 2008. European storminess: late nineteenth century to present. *Clim. Dyn.* **31**: 125–130.

Mesquita MDS, Gunnar Kvamstø N, Sorteberg A, Atkinson DE. 2008. Climatological properties of summertime extra-tropical storm tracks in the Northern Hemisphere. *Tellus A* **60**: 557–569.

Murphy SJ, Washington R. 2001. United Kingdom and Ireland precipitation variability and the North Atlantic sea-level pressure field. *Int. J. Climatol.* **21**: 939–959.

Murphy C, Harrigan S, Hall J, Wilby RL. 2013. Climate-driven trends in mean and high flows from a network of reference stations in Ireland. *Hydrol. Sci. J.* **58**: 755–772.

Neu U, Akperov MG, Bellenbaum N, Benestad R, Blender R, Caballero R, Cocozza A, Dacre HF, Feng Y, Fraedrich K, Grieger J, Gulev S, Hanley J, Hewson T, Inatsu M, Keay K, Kew SF, Kindem I, Leckebusch GC, Liberato MLR, Lionello P, Mokhov II, Pinto JG, Raible CC, Reale M, Rudeva I, Schuster M, Simmonds I, Sinclair M, Sprenger M, Tilinina ND, Trigo IF, Ulbrich S, Ulbrich U, Wang XL, Wernli H. 2013. Imilast: a community effort to intercompare extratropical cyclone detection and tracking algorithms. *Bull. Am. Meteorol. Soc.* **94**: 529–547.

Parry S, Marsh T, Kendon M. 2013. 2012: from drought to floods in England and Wales. *Weather* **68**: 268–274.

Pattison I, Lane SN. 2012. The relationship between Lamb weather types and long-term changes in flood frequency, River Eden, UK. *Int. J. Climatol.* **32**: 1971–1989.

Raible CC, Della-Marta PM, Schwierz C, Wernli H, Blender R. 2008. Northern Hemisphere extratropical cyclones: a comparison of detection and tracking methods and different reanalyses. *Mon. Weather Rev.* **136**: 880–897.

Rodda JC, Marsh TJ. 2011. *The 1975-76 Drought – A Contemporary and Retrospective Review*. National Hydrological Monitoring Programme Series. NERC/Centre for Ecology and Hydrology: Wallingford, UK.

Scherrer SC, Croci-Maspoli M, Schwierz C, Appenzeller C. 2006. Two-dimensional indices of atmospheric blocking and their statistical relationship with winter climate patterns in the Euro-Atlantic region. *Int. J. Climatol.* **26**: 233–249.

Sen PK. 1968. Estimates of the regression coefficient based on Kendall's tau. *J. Am. Stat. Assoc.* **63**: 1379–1389.

Serreze MC, Barrett AP. 2008. The summer cyclone maximum over the central Arctic Ocean. *J. Climatol.* **21**: 1048–1065.

Simmonds I, Keay K. 2000. Mean Southern Hemisphere extratropical cyclone behavior in the 40-year NCEP-NCAR reanalysis. *J. Climatol.* **13**: 873–885.

Smits A, Klein Tank AMG, Können GP. 2005. Trends in storminess over the Netherlands, 1962–2002. *Int. J. Climatol.* **25**: 1331–1344.

Sweeney J. 2000. A three-century storm climatology for Dublin 1715–2000. *Irish Geogr.* **33**: 1–14.

Theil H. 1950. A rank-invariant method of linear and polynomial regression analysis I. *Nederlands Akad. Wetensch. Proc.* **53**: 386–392.

Tibaldi S, Molteni F. 1990. On the operational predictability of blocking. *Tellus A* **42**: 343–365.

Trigo RM, Osborn TJ, Corte-Real JM. 2002. The North Atlantic Oscillation influence on Europe: climate impacts and associated physical mechanisms. *Clim. Res.* **20**: 9–17.

Vilibic I, Sepic J. 2010. Long-term variability and trends of sea-level storminess and extremes in European Seas. *Glob. Planet. Change* **71**: 1–12.

Wang XL, Swail VR, Zwiers FW. 2006. Climatology and changes of extratropical cyclone activity: comparison of ERA-40 with NCEP-NCAR reanalysis for 1958-2001. *J. Climatol.* **19**: 3145–3166.

Wang XL, Zwiers FW, Swail VR, Feng Y. 2009. Trends and variability of storminess in the Northeast Atlantic region, 1874–2007. *Clim. Dyn.* **33**: 1179–1195.

Wang XL, Wan H, Zwiers FW, Swail VR, Compo GP, Allan VRS, Jourdain S, Yin X. 2011. Trends and low-frequency variability of storminess over western Europe, 1878–2007. *Clim. Dyn.* **37**: 2355–2371.

Wang XL, Feng Y, Compo GP, Swail VR, Zwiers FW, Allan RJ, Sardeshmukh PD. 2013. Trends and low frequency variability of extra-tropical cyclone activity in the ensemble of twentieth century reanalysis. *Clim. Dyn.* **40**: 2775–2800.

Wang XL, Feng Y, Compo GP, Zwiers FW, Allan RJ, Swail VR, Sardeshmukh PD. 2014. Is the storminess in the Twentieth Century

Reanalysis really inconsistent with observations? A reply to the comment by Krueger et al. (2013b). *Clim. Dyn.* **42**: 1113–1125.

Wilby RL, Quinn NW. 2013. Reconstructing multi-decadal variations in fluvial flood risk using atmospheric circulation patterns. *J. Hydrol.* **487**: 109–121.

Wilby RL, O'Hare G, Barnsley N. 1997. The North Atlantic Oscillation and British Isles climate variability, 1865–1996. *Weather* **52**: 266–276.

Wilby RL, Conway D, Jones PD. 2002. Prospects for downscaling seasonal precipitation variability using conditioned weather generator parameters. *Hydrol. Processes* **16**: 1215–1234.

Woodworth PL, Blackman DL. 2002. Changes in extreme high waters at Liverpool since 1768. *Int. J. Climatol.* **22**: 697–714.

Woollings T. 2010. Dynamical influences on European climate: an uncertain future. *Philos. Trans. R. Soc. A* **368**: 3733–3756.

Woollings T, Hoskins B, Blackburn M, Berrisford P. 2008. A new Rossby wave-breaking interpretation of the North Atlantic Oscillation. *J. Atmos. Sci.* **65**: 609–626.

Woollings T, Gregory JM, Pinto JG, Reyers M, Brayshaw DJ. 2012. Response of the North Atlantic storm track to climate change shaped by ocean-atmosphere coupling. *Nat. Geosci.* **5**: 313–317.

Zappa G, Shaffrey LC, Hodges KI, Sansom PG, Stephenson DB. 2013. A multimodel assessment of future projections of North Atlantic and European extratropical cyclones in the CMIP5 climate models. *J. Clim.* **26**: 5846–5862, doi: 10.1175/JCLI-D-12-00573.1.